1 Dissociable neural information dynamics of perceptual integration
2 and differentiation during bistable perception

3

4   Andrés **Canales-Johnson**[1,2*], Alexander J. **Billig**[3,4], Francisco **Olivares**[5], Andrés **Gonzalez**[5], María del

5   Carmen **Garcia**[6], Walter **Silva**[6], Esteban **Vaucheret**[6], Carlos **Ciraolo**[6], Ezequiel **Mikulan**[7], Agustín

6   **Ibanez**[7,8,9,10,11], David **Huepe**[10], Srivas **Chennu**[12,13] and Tristan A. **Bekinschtein**[1]

7

8   1 Department of Psychology, University of Cambridge, Cambridge, United Kingdom.

9   2 Vicerectoria de Investigacion y Posgrado, Universidad Catolica del Maule, Talca, Chile.

10   3 Brain and Mind Institute, University of Western Ontario, London, Canada.

11   4 UCL Ear Institute, University College London, London, United Kingdom

12   5 Facultad de Psicologia, Universidad Diego Portales, Chile.

13   6 Programa de Cirugía de Epilepsia, Hospital Italiano de Buenos Aires, Argentina.

14   7 Laboratory of Experimental Psychology and Neuroscience (LPEN), Institute of Cognitive and
15   Translational Neuroscience (INCyT), INECO Foundation, Favaloro University, Buenos Aires, Argentina.

16   8 National Scientific and Technical Research Council (CONICET), Buenos Aires, Argentina.

17   9 Universidad Autónoma del Caribe, Barranquilla, Colombia

18   10 Center for Social and Cognitive Neuroscience (CSCN), School of Psychology, Universidad Adolfo
19   Ibáñez, Santiago, Chile.

20   11 Centre of Excellence in Cognition and its Disorders, Australian Research Council (ACR), Sydney,
21   Australia.

22   12 School of Computing, University of Kent, Chatham Maritime, United Kingdom.

23   13 Department of Clinical Neurosciences, University of Cambridge, United Kingdom.

24

25   * Correspondence:

26   Andres Canales-Johnson, PhD

27   Department of Psychology

28   University of Cambridge

29   Downing Site, CB2 3EB

30   Cambridge, United Kingdom.

31   afc37@cam.ac.uk

32

33 **Author's contributions**

34 Conceived and designed the experiments: ACJ, TAB. Performed the experiments: ACJ, FO, AG, EM.
35 Analysed the data: ACJ. Contributed reagents/materials/analysis tools: AB, DH, SC. Gave access to
36 clinical patient: MCG, WS, EV, CC. Wrote the paper: ACJ, AB, AI, SC, TAB.

37 **Acknowledgments**

38 We thank Robert Carlyon, Simon van Gaal, Jean-Phillippe Lachaux, Anat Arzi, William J. Harrison,
39 Daniel Bor and Victor Lamme for contributing to valuable discussion and insights. This manuscript is
40 dedicated to the memory of Prof. Walter J. Freeman (1927 - 2016) whose pioneering work on
41 Neurodynamics has inspired and ignited countless meaningful insights during the execution of this
42 project.

43 **Funding**

44 This research was supported by a Wellcome Trust Biomedical Research Fellowship WT093811MA
45 and the Chilean National Fund for Scientific and Technological Development Grant 1171200.

46 **Conflict of Interest**

47 None declared.

48

49

50

51

52

53

54

55

56

57

58

59

60   **ABSTRACT**

61   At any given moment, we experience a perceptual scene as a single whole and yet we may

62   distinguish a variety of objects within it. This phenomenon instantiates two properties of

63   conscious perception: integration and differentiation. Integration to experience a collection of

64   objects as a unitary percept, and differentiation to experience these objects as distinct from each

65   other. Here we evaluated the neural information dynamics underlying integration and

66   differentiation of perceptual contents during bistable perception. Participants listened to a

67   sequence of tones (auditory bistable stimuli) experienced either as a single stream (perceptual

68   integration) or as two parallel streams (perceptual differentiation) of sounds. We computed

69   neurophysiological indices of information integration and information differentiation with

70   electroencephalographic and intracranial recordings. When perceptual alternations were

71   endogenously driven, the integrated percept was associated with an increase in neural

72   information-integration and a decrease in neural differentiation across frontoparietal regions,

73   whereas the opposite pattern was observed for the differentiated percept. However, when

74   perception was exogenously driven by a change in the sound stream (no bistability) neural

75   oscillatory power distinguished between percepts but information measures did not. We

76   demonstrate that perceptual integration and differentiation can be mapped to theoretically-

77   motivated neural information signatures, suggesting a direct relationship between

78   phenomenology and neurophysiology.

79

82

83

84

85

86

87

88

89

90

91   **INTRODUCTION**

92   Phenomenologically, conscious experience does not only depend on the external information we
93   receive from the environment, but also on internal information that is independent of sensory
94   stimulation. This dissociation between external stimulation and conscious experience is observed in
95   several visual and auditory perceptual illusions in which two or more internally driven percepts
96   alternate under unchanging external stimulation (Sterzer et al. 2009). Moreover, conscious
97   experience cannot be divided into discrete independent components (i.e., it is perceptually
98   integrated), but it can contain an assortment of events and objects (i.e., it is perceptually
99   differentiated) (Tononi et al. 2016). Thus, while integration is the property of experiencing a
100   collection of objects as a unitary percept, differentiation is the property of experiencing these
101   objects as distinct from each other. What are the neural markers of the integration and
102   differentiation of internally driven perceptual contents? We propose that integration and
103   differentiation of internally driven percepts can be neurophysiologically investigated during auditory
104   bistability. During the particular form of auditory bistability employed here, an invariant sequence of
105   tones is experienced as forming either an integrated percept (one stream) or a differentiated
106   percept (two streams) (Snyder et al. 2012) (Figure 1).

107   Neurophysiologically, conscious experience is thought to require the joint presence of information
108   integration and information differentiation (Fahrenfort et al., 2012; Oizumi et al. 2014; Tononi et al.
109   2016; Fahrenfort et al., 2017). In particular, the emergence of conscious percepts is believed to
110   involve the integration of information coming from frontal and parietal brain areas to form a
111   phenomenologically unified whole (Dehaene and Changeux 2011; Dehaene et al. 2014; Tononi et al.
112   2016). Therefore, a reasonable assumption is that the integrated percept (one stream, in the case of
113   this experiment) should be associated with correspondingly higher neural information integration
114   (NII). Recently, NII has been empirically measured in a direct manner by computing the amount of
115   information shared between long-distance EEG signals, and it has been used to discriminate
116   between vegetative and minimally conscious patients (King et al. 2013; Sitt et al. 2014). This NII
117   measure can detect non-oscillatory coupling between signals as compared to classical measures of
118   neural oscillatory integration (NOI) such as phase synchronization. In the case of auditory bistability,
119   we expect higher neural information integration for the perceptually integrated (one-stream)
120   percept compared to the perceptually differentiated (two-stream) percept, as the former would
121   require information about tones of two different frequencies to form a single, integrated percept.

122   Complementary to NII, empirical indices of neural information differentiation (NID) have been used

123   to separate levels of consciousness by estimating the degree of compressibility of EEG signals (Casali

124   et al. 2013; Sitt et al. 2014; Schartner et al. 2015, 2017). For instance, a decrease in NID has been

125   observed in patients in vegetative states compared to minimally conscious states (Sitt et al. 2014),

126   showing that differentiation of neural information is associated with a cognitively more advanced

127   state of consciousness, as clinically defined. On the other hand, the only study providing a

128   preliminary indication that neurophysiological differentiation might be related to perceptual

129   processes is an fMRI study (Boly et al. 2015), showing that NID was highest when participants

130   watched a coherent movie, intermediate when scenes were scrambled, and minimal for 'TV noise'.

131   However, it is unclear whether neurophysiological differentiation was specifically related to

132   conscious awareness since factors such as low-level visual processing, expectations and top-down

133   attention might have influenced the differences observed between conditions. During auditory

134   bistability, we can specifically evaluate perceptual differentiation directly since what is changing is

135   not the stimulus itself but how it is subjectively experienced. If the neural information associated

136   with a conscious percept is highly differentiated, NID is expected to be high since information should

137   be less compressible. In contrast, neural differentiation is expected to be low if EEG signals are

138   processing information in a stereotypical way because information is highly redundant (easily

139   compressed). Following this rationale, we expect that the differentiated (two-stream) percept

140   should be associated with higher neural information differentiation.

141   In addition, there is ample and rapidly growing evidence that endogenous or 'ongoing' brain activity

142   in the gamma band (30-70 Hz) is neither meaningless nor random but instead carries functional

143   information largely determining the way incoming stimuli are interpreted (Engel et al. 2001, 2013;

144   Varela et al. 2001; Freeman 2015). For instance, studies of the visual system have shown that neural

145   oscillatory integration (NOI) in the gamma band is involved in the alternation between visual

146   conscious percepts (Doesburg et al. 2005; Hipp et al. 2012). Thus, drawing upon these results and a

147   wealth of previous research that has identified gamma band activity as relevant for conscious

148   perception (Melloni et al. 2007; Engel et al. 2013; Levy et al. 2015), here we analyse information and

149   oscillatory dynamics of ongoing activity in the gamma band. However, we specifically evaluate the

150   theoretical prediction (Koch et al. 2016) that information dynamics (NII and NID) but not oscillatory

151   dynamics (NOI) of ongoing activity underpin phenomenological integration and differentiation.

152   By measuring high-density scalp EEG and intracranial EEG (iEEG) in humans, we tested the

153   hypothesis that during the formation of internally driven percepts, conscious experience goes along

154   with neurophysiological indices of information processing. Specifically, we predicted that the

155   perceptually integrated content would correspond to high frontoparietal neural information

156   integration in the gamma band and conversely, the perceptually differentiated content would be

157   associated with high neural information differentiation within frontal and parietal regions.

158   **Materials and Methods**

159   **Healthy participants and patient**

160   Twenty-nine right-handed healthy participants (14 males; mean ± SD age = 21.30 ± 2.2 years) and

161   one left-handed epileptic patient (female; 29 years) gave written informed consent to take part in

162   the experiment. The study was approved by the institutional ethics committee of the Faculty of

163   Psychology of Universidad Diego Portales (Chile) and the Institutional Ethics Committee of the

164   Hospital Italiano de Buenos Aires, Argentina, in accordance with the Declaration of Helsinki. The

165   patient suffered from drug-resistant epilepsy from the age of 8 years and was offered surgical

166   intervention to alleviate her intractable condition. Drug treatment at the time of implantation

167   included 600 mg/d oxcarbazepine, 200 mg/d topiramate, and 750 mg/d levetiracetam. Computed

168   tomography (CT) and magnetic resonance imaging (MRI) scans were acquired after insertion of

169   depth electrodes. The patient took part in the current study one day before the surgery. She was

170   attentive and cooperative during testing, and her cognitive performance before and one week after

171   the implantation was indistinguishable from healthy volunteers. The patient was specifically

172   recruited for this study because she was implanted with electrodes covering frontal and parietal

173   regions (Table 1). Healthy participants and the epileptic patient performed the task with eyes closed

174   in a dimly lit room.

175   **Stimuli and experimental conditions**

176   There were two experimental conditions. In the endogenous condition (bistability), we used a

177   bistable auditory tone sequence (Carlyon et al. 2001; Gutschalk et al. 2005; Pressnitzer and Hupé

178   2006). Participants listened to a repeating pattern of three tones (ABA), each group of which was

179   followed by a silence ('-'); the pattern is experienced either as a one-stream percept or as a two-

180   stream percept (Figure 1A). The frequency of the A tone was 587 Hz and that of the B tone was 440

181   Hz (5 semitones difference). The duration of each tone was 120 ms. The silence ('-') that completed

182   the ABA… pattern was also 120 ms long, thus making both the set of A tones and the set of B tones

183   isochronous (Pressnitzer and Hupé 2006). Participants were instructed to press a button with one

184   hand when perceiving that the one-stream percept had fully changed into two streams and a second

185   button with the other hand when perceiving that the two-stream percept had fully changed into one

186   stream (Figure 1A, middle panel).

187   In the exogenous condition (control), participants listened to repeating patterns of three (ABA) or

188   two (AB) tones, each group of which was separated by one ('-') or two periods of silence ('--')

189   respectively. In both cases the A and B tones had the same parameters (frequencies and duration)

190   and the silence had the same duration as in the endogenous condition (ABA- pattern). In the

191   exogenous condition blocks of each pattern (ABA- and AB--) were constructed to last 4-8 seconds

192   before changing to the other pattern. This suppressed the effect of endogenous bistability, such that

193   ABA- was most often perceived as one stream, whereas AB-- was largely perceived as two streams.

194   As in the endogenous conditions, participants were instructed to press a button with one hand when

195   perceiving that ABA- had fully changed into AB-- and another button with the other hand when

196   pattern AB-- had fully changed into ABA-. Importantly, the exogenous condition allowed us to

197   characterize the dynamics of neural activity specifically related to external changes in the stimuli

198   (the two alternating patterns) and to contrast them with the dynamics of internal neural activity

199   elicited by the endogenous condition (bistability). The endogenous and exogenous conditions used

200   physically similar stimuli, with the latter sometimes having one fewer A tone. Because the analysis

201   windows were not time-locked to the stimuli, but rather to responses (see "Analysis of ongoing

202   neural activity"), differences in the evoked responses to specific tones are unlikely to account for the

203   observed pattern of results.

204   In order to match both conditions as closely as possible, the exogenous condition was always

205   preceded by the endogenous condition. By designing the experiment in this manner, we were able

206   to quickly calculate the number of both types of alternations during the endogenous conditions on a

207   participant-per-participant basis. Based on this individual calculation, we structured the subsequent

208   exogenous condition based on the number of switches of the endogenous condition. Similarly, the

209   pattern of alternation (i.e. stimuli sequence) in the exogenous conditions was defined based on the

210   first switch observed during the endogenous condition (i.e. the sequence started either with a one-

211   stream stimulus or with a two-stream stimulus). This procedure was meant to control for differences

212   in the number of alternations and for differences in the sequence of alternations between

213   conditions.

214   **Electroencephalography (EEG) recordings, pre-processing and analysis**

215   EEG signals were recorded with 128-channel HydroCel Sensors using a GES300 Electrical Geodesic

216   amplifier at a sampling rate of 500 Hz using the NetStation software. During recording and analyses,

217   the electrodes' average was used as the reference electrode. Two bipolar derivations were designed

218   to monitor vertical and horizontal ocular movements. Following Chennu *et al* (Chennu et al. 2014),

219   data from 92 channels over the scalp surface were retained for further analysis. Channels on the

220   neck, cheeks and forehead, which reflected more movement-related noise than signal, were

221   excluded. Eye movement contamination, cardiac and muscle artefacts were removed from data

222   before further processing using an independent component analysis (ICA) (Delorme and Makeig

223   2004). All conditions yielded at least 91% of artefact-free trials. Trials (-2500 to 0 ms relative to a

224   button press) that contained voltage fluctuations exceeding ±200 μV or transients exceeding

225   ±100 μV were also excluded. The EEGLAB MATLAB toolbox was used for data pre-processing and

226   pruning (Delorme and Makeig 2004). MATLAB open source software FieldTrip (Oostenveld et al.

227   2011) and customized scripts were used for calculating Neural Information Integration (NII), Neural

228   Information Differentiation (NID), Neural Oscillatory Integration (NOI) and Neural Oscillatory Power

229   (NOP) measures. No filtering was performed during the pre-processing stage.

230   **Intracranial electroencephalography (iEEG): recordings and pre-processing**

231   Stereo-electroencephalography (SEEG), an intracranial electroencephalography (iEEG) recording

232   technique in which depth electrodes are inserted in the brain of epileptic patients, were obtained

233   from semi-rigid, multi-lead electrodes implanted in a single patient. The electrodes had a diameter

234   of 0.8 mm and consisted of 5, 10 or 15 contact leads that were 2-mm wide and 1.5-mm apart (DIXI

235   Medical Instruments). The electrode shafts were implanted in different regions of the frontal,

236   temporal, central and parietal cortices and subcortical structures. For the purposes of the current

237   study, iEEG recordings were analysed from the left orbitofrontal cortex (OF), left middle frontal gyrus

238   (MFG), left superior parietal lobe (SPL), left primary motor cortex (MC) and left posterior insular

239   cortex (PIC) (Table 1). Each electrode located in grey matter was re-referenced to an electrode of the

240   same electrode shaft located in white matter (Li et al., 2018). Following this procedure, we

241   preserved the limited number of electrodes in SPL (2 electrodes), OF (3 electrodes) and MFG (3

242   electrodes) that would have been reduced in number using a bipolar reference (N-1). MNI

243   coordinates of the depth electrodes were obtained from MRI and CT images using SPM (Friston

244   2006) and MRIcron (Rorden and Brett 2000) software. The recordings were sampled at 1024 Hz and

245   down-sampled to 500 Hz for further analysis. The exact MNI coordinates and cortical regions of the

246   selected electrodes are reported in Table 1. Open-source BrainNet Viewer software was used for

247   visualization of selected electrodes (Xia et al. 2013).

248   **Analysis of ongoing neural activity**

249   A classical experimental approach for studying endogenous, or "ongoing" activity in the EEG related

250   to internal fluctuations during cognitive tasks is by analysing the EEG window before the onset of

251   motor responses when participants report internal changes. This approach has been used for

252   studying neural signatures of conscious awareness, such as in bistable perception (Parkkonen et al.

253 2008), binocular rivalry (Doesburg et al. 2005; Frässle et al. 2014) and intrusions of consciousness

254 (Noreika et al. 2015). Here, ongoing EEG and iEEG activity (not time-locked to stimuli) preceding the

255 onset of each response (button press), and presumed to span the change in perception, was

256 analysed in terms of connectivity (NII and NOI) and complexity (NII).

257 Window size selection was based on the following procedure. First, we calculated the mean reaction

258 time in the exogenous condition (M = 1342 ms; SD = 101 ms). Second, in the endogenous condition,

259 we calculated the minimum inter-switch duration such that windows would not overlap after EEG

260 data epoching (the minimum window size was 2500 ms; epoching from -2500 to 0 ms relative to

261 button press). Third, as the mean RT in the exogenous condition (1342 ms) was approximately half of

262 the window size of the endogenous condition (2500 ms), we selected a window of analysis of 2500

263 ms for both conditions (from -2500 to 0 ms relative to button press) (Figure 1, lower panel).

264 Importantly, this window included the onset of the exogenous auditory patterns ('ABA-' and 'AB--').

265 The same procedure was repeated for the intracranial patient (reaction times in the exogenous

266 condition: M = 1380 ms, SD = 79 ms; window size in the endogenous conditions: 2500 ms).

267 For statistical analyses (see below), two time windows of 500 ms were selected based on the

268 exogenous condition. A window after the change between auditory percepts (after-change window

269 (AC)) was defined based on the mean reaction time at the group level (from -1342 to -842 ms). A

270 second time window was defined at the epoch onset (before-change window (BC); from -2500 to -

271 2000 ms). The rationale behind the latencies of both time windows was to select *a priori* the periods

272 when both externally driven percepts remained perceptually stable. Windows were not selected

273 using a data-driven approach (see Supplementary Figure 1). The same window lengths and latencies

274 were used for the endogenous condition (Figure 1).

275 **Neural oscillatory power (NOP): spectral power**

276 In order to derive our measure of neural oscillatory power, we first band-pass filtered the raw signal

277 using a 6th order Butterworth filter. Spectral power was estimated by calculating the square of the

278 envelope obtained from the absolute value of the Hilbert transform after filtering. This procedure

279 provides the instantaneous power emission which reflects the strength of local synchronization. The

280 frequency bands were defined as follows: theta (4–7 Hz), alpha (8–12 Hz), beta (15–25 Hz), gamma

281 (30–60 Hz), following the canonical frequency-band classification (e.g. Li et al., 2018).

282 **Phase synchronization**

283 We quantified phase coherence between pairs of electrodes as a measure of dynamical linear
284 coupling among signals oscillating in the same frequency band. Phase synchronization analysis
285 proceeds in two steps: (i) estimation of the instantaneous phases and (ii) quantification of the phase
286 locking.

287

288

289 **Estimation of the instantaneous phases**

290 To obtain the instantaneous phases φ of the neural signals, we used the Hilbert transform approach
291 (Foster et al. 2016). The analytic signal $\xi(t)$ of the univariate measure $x(t)$ is a complex function of
292 continuous time t defined as:

293 $$(1) \quad \xi(t) = x(t) + ix_h(t) = a_\xi(t)e^{i\varphi_\xi(t)}$$

294 where the function $x_h(t)$ is the Hilbert transform of $x(t)$:

295 $$(2) \quad x_h(t) = \frac{1}{\pi}P.V. \int_{-\infty}^{+\infty}\frac{x(t)}{t-\tau}d\tau$$

296 P.V. indicates that the integral is taken in the sense of Cauchy principal value. Sequences of digitized
297 values give a trajectory of the tip of a vector rotating counterclockwise in the complex plane with
298 elapsed time.

299 The vector norm at each digitizing step t is the state variable for instantaneous amplitude $a_\xi(t)$. This
300 amplitude corresponds to the length of the vector specified by the real and imaginary part of the
301 complex vector computed by Pythagoras' law and is equivalent to the magnitude of the observed
302 oscillation at a given time and frequency point.

303 $$(3) \quad a_\xi(t) = \sqrt{x(t)^2 + ix_h(t)^2}$$

304 and the arctangent of the angle of the vector with respect to the real axis is the state variable for
305 instantaneous phase $\varphi_x(t)$.

306 $$(4) \quad \varphi_x(t) = arctg\frac{ix_h(t)}{x(t)}$$

307 The instantaneous phase $\varphi_x(t)$ of $x(t)$ is taken equal to $\varphi_\xi(t)$. Identically, the phase $\varphi_y(t)$ is estimated
308 from $y(t)$. This phase is thus the angle of the vector specified by the real and imaginary components.

309   For a given time and frequency point, it corresponds to a position inside the oscillation cycle (peak,

310   valley, rising, or falling slope).

311   The instantaneous phase, although defined uniquely for any kind of signal to which the Hilbert

312   transform can be applied, is difficult to interpret physiologically for broadband signals. For this

313   reason, a standard procedure is to consider only narrow-band phase synchronization by estimating

314   an instantaneous phase for successive frequency bands, which are defined by band-pass filtering the

315   time series (Le Van Quyen et al. 2001). Thus, for each trial and electrode, the instantaneous phase of

316   the signal was extracted at each frequency of the interval 1- 60 Hz (in 1-Hz steps) by computing the

317   Hilbert transform using a zero phase shift non-causal finite impulse filter.

318   **Neural oscillatory integration (NOI): weighted phase lag index (wPLI)**

319   Phase synchronization is often calculated from the phase or the imaginary component of the

320   complex cross-spectrum between the signals measured at a pair of channels. For example, the well-

321   known Phase Locking Value (PLV) (Lachaux et al. 1999) is obtained by averaging the exponential

322   magnitude of the imaginary component of the cross-spectrum. However, such phase coherence

323   indices derived from EEG data are affected by the problem of volume conduction, and as such they

324   can have a single dipolar source, rather than a pair of distinct interacting sources, producing spurious

325   coherence between spatially disparate EEG channels. The Phase Lag Index (PLI), first proposed by

326   Stam *et al* (Stam et al. 2007) attempts to minimize the impact of volume conduction and common

327   sources inherent in EEG data, by averaging the signs of phase differences, thereby ignoring average

328   phase differences of 0 or 180 degrees. This is based on the rationale that such phase differences are

329   likely to be generated by volume conduction of single dipolar sources. However, despite being

330   insensitive to volume conduction, PLI has a strong discontinuity in the measure, which causes it to be

331   maximally sensitive to noise.

332   The Weighted Phase Lag Index (wPLI) (Vinck et al. 2011) addresses this problem by weighting the

333   signs of the imaginary components by their absolute magnitudes. Further, as the calculation of wPLI

334   also normalises the weighted sum of signs of the imaginary components by the average of their

335   absolute magnitudes, it represents a dimensionless measure of connectivity that is not directly

336   influenced by differences in spectral or cross-spectral power. For these reasons, we employed the

337   wPLI measure to estimate connectivity in our data. The wPLI index ranges from 0 to 1, with value 1

338   indicating perfect synchronization (phase difference is perfectly constant throughout the trials) and

339   value 0 representing total absence of synchrony (phase differences are random). For each trial and

340   pair of electrodes, wPLI was estimated using a 500 ms sliding window with 2 ms time step, i.e. with a

341   96% overlap between two adjacent windows.

342   **Neural information integration (NII): weighted symbolic mutual information (wSMI)**

343   In order to quantify the coupling of information flow between electrodes we computed the

344   weighted symbolic mutual information (wSMI) (King et al. 2013; Sitt et al. 2014). This measure

345   assesses the extent to which two signals present joint non-random fluctuations, suggesting that they

346   share information. wSMI has three main advantages: (i) it allows for a rapid and robust estimation of

347   the signals' entropies; (ii) it provides an efficient way to detect non-linear coupling; and (iii) it

348   discards spurious correlations between signals arising from common sources, favouring non-trivial

349   pairs of symbols. For each trial, wSMI is calculated between each pair of electrodes after the

350   transformation of the EEG and iEEG signals into a sequence of discrete symbols defined by the

351   ordering of k time samples separated by a temporal separation τ (King et al. 2013). The symbolic

352   transformation depends on a fixed symbol size (k = 3, that is, 3 samples represent a symbol) and a

353   variable τ between samples (temporal distance between samples) which determines the frequency

354   range in which wSMI is estimated (Sitt et al. 2014). In our case, we chose τ = 32 and 6 ms to isolate

355   wSMI in alpha ($wSMI_\alpha$) and gamma ($wSMI_v$) bands respectively. The frequency specificity f of wSMI is

356   related to k and τ as:

357

358    $$f = 1000 / (\tau * k)$$

359

360   As per the above formula, with a kernel size k of 3, τ values of 32 and 6 ms produced a sensitivity to

361   frequencies below and near to 55 Hz (gamma range) and 10 Hz (alpha range), respectively, with

362   these two frequency values used as low-pass filters in order to avoid aliasing artifacts (King et al.,

363   2013)

364

365   wSMI was estimated for each pair of transformed EEG and iEEG signals by calculating the joint

366   probability of each pair of symbols. The joint probability matrix was multiplied by binary weights to

367   reduce spurious correlations between signals, as confirmed by simulations and empirical data in the

368   original wSMI publication (King et al., 2013). The weights were set to zero for pairs of identical

369   symbols, which could be elicited by a unique common source, and for opposite symbols, which could

370   reflect the two sides of a single electric dipole. wSMI is calculated using the following formula:

371

$$wSMI(X,Y) = \frac{1}{\log(k!)} \sum_{x \in X} \sum_{y \in Y} w(x,y)\, p(x,y) \log\left(\frac{p(x,y)}{p(x)p(y)}\right)$$

372

373   where *x* and *y* are all symbols present in signals *X* and *Y* respectively, w*(x,y)* is the weight matrix and

374   *p(x,y)* is the joint probability of co-occurrence of symbol *x* in signal *X* and symbol *y* in signal *Y*. Finally,

375   *p(x)* and *p(y)* are the probabilities of those symbols in each signal and *k* is the number of symbols -

376   used to normalize the mutual information (MI) by the signal's maximal entropy. Temporal evolution

377   of wSMI was calculated using a 500 ms sliding window with 2 ms time step, i.e. with a 96% overlap

378   between two adjacent windows.

379

380   In order to further address possible volume conduction issues in our scalp EEG analyses, we

381   compared wSMI with the non-weighted versions of the metric (Symbolic Mutual Information; SMI),

382   computing both metrics as a function of Euclidean inter-electrode distance (Supplementary Figure

383   7). For distances below 5 cm, wSMI quickly dropped toward zero, as expected given that the

384   weighted version of this measure was designed to eliminate common source artifacts and to provide

385   higher spatial selectivity (King et al., 2013) (Supplementary Figure 7, *upper row*). In contrast, the

386   unweighted version of the metric (SMI) exhibited the highest values below 5 cm, typically produced

387   by common source artifacts (Supplementary Figure 7, *lower row*). These analyses further confirm

388   that the differences observed in our data are most likely due to a non-spurious spatial relationship

389   between electrode pairs.

390

391   **Neural information differentiation (NID): Kolmogorov-Chaitin complexity (K complexity)**

392   Kolmogorov-Chaitin complexity quantifies the algorithmic complexity (Kolmogorov 1965; Chaitin

393   1974) of an EEG signal by measuring its degree of redundancy (Sitt et al. 2014; Schartner et al. 2015,

394   2017). Algorithmic complexity of a given EEG sequence can be described as the length of shortest

395   computer program that can generate it. A short program corresponds to a less complex sequence. K

396   complexity was estimated by quantifying the compression size of the EEG using the Lempel-Ziv zip

397   algorithm (Lempel and Ziev 1976).

398   Algorithmic information theory was introduced by Andreï Kolmogorov and Gregory Chaitin as an

399   area of interaction between computer science and information theory. The concept of algorithmic

400   complexity or Kolmogorov-Chaitin complexity (K complexity) is defined as the shortest description of

401   a string (or in our case a time series *X*). That is to say, K complexity is the size of the smallest

402   algorithm (or computer program) that can produce that particular time series. However, it can be

403   demonstrated by *reductio ad absurdum* that there is no possible algorithm that can measure K

404   complexity (Chaitin 1995). To sidestep this issue, we can estimate an upper-bound value of K

405   complexity(X). This can be concretely accomplished by applying a lossless compression of the time

406   series and quantifying the compression size. Capitalizing on the vast signal compression literature,

407   we heuristically used a classical open-source compressor gzip (Salomon 2004) to estimate K

408   complexity(X). It is important to standardize the method of representation of the signal before

409   compression in order to avoid non-relevant differences in complexity. Specifically, to compute K

410   complexity(X):

1.   The time series were transformed into sequences of symbols. Each symbol represents, with
      identical complexity, the amplitude of the corresponding channel for each time point. The
      number of symbols was set to 32 and each one corresponds to dividing the amplitude range
      of that given channel into 32 equivalent bins. Similar results have been obtained with
      binning ranging from 8 to 128 bins (Sitt et al. 2014).

2.   The time series were compressed using the compressLib library for Matlab, this library
      implements the gzip algorithm to compress Matlab variables.

3.   K complexity(X) was calculated as the size of the compressed variable with time series
      divided by the size of the original variable before compression. Our premise is that, the
      larger the size of the compressed string, the more complex the structure of the time series,
      thus potentially indexing the complexity of the electrical activity recorded at a sensor.

422   For each trial and channel, K complexity was estimated using a 500 ms sliding window with 2 ms

423   time step, i.e. with a 96% overlap between two adjacent windows.

424   **EEG electrode cluster analysis and epoch correction**

425   For the hypothesis-driven analyses, canonical bilateral frontal (n=26), parietal (n=18), and temporal

426   (n=12) electrode clusters were selected for spectral power, complexity (K-complexity) and

427   connectivity analysis (wPLI and wSMI) (Supplementary Figure 14). In the case of spectral power and

428   complexity analysis, values within frontal and parietal electrode clusters were averaged per

429   condition and participant. In the case of frontoparietal wPLI, wSMI, we calculated the mean

430   connectivity that every electrode in the frontal cluster shared with every electrode in the parietal

431   cluster. In order to evaluate long-distance interactions between frontal and parietal electrodes,

432   values between pairs of frontal electrodes and between pairs of parietal electrodes were discarded.

433   Similarly, in the case of temporotemporal connectivity analyses, we calculated the mean

434   connectivity that every electrode in the right-temporal cluster shared with every electrode in the

435   left-temporal cluster, discarding connectivity values within pairs of right-temporal electrodes and

436   pairs of left-temporal electrodes. This procedure allowed us to specifically test the role of long-

437   distance interactions (frontoparietal and temporotemporal) during the endogenous and exogenous

438   conditions. Spectral power, K complexity, wSMI and wPLI values of the corresponding regions of

439   interest were averaged per condition and participant. For the exploratory analysis, connectivity

440   between pairs of frontal and pairs of parietal electrodes were analysed separately. In a similar

441   manner as for the hypothesis-driven analysis, connectivity (wSMI) between frontotemporal and

442   temporoparietal electrodes were analysed, within-cluster pairs were excluded.

443   Since during the endogenous condition there was no true baseline period because we do not know

444   precisely when the spontaneous changes were initiated, after transforming data into complexity (K

445   complexity), connectivity (wPLI and wSMI) and spectral power time series, and creating the

446   corresponding electrode clusters, we subtracted the mean values between -2500 and -700 ms from

447   each data point per epoch and condition. Motor-related activity in the gamma band has been

448   reported ~-200 ms before the button press during auditory bistable perception (Basirat et al. 2008).

449   Thus, although it is common to analyse response-evoked activity by normalizing epochs using the

450   mean of the entire window including the time of the motor response (Doesburg et al. 2005; Fesi and

451   Mendola, 2014; de Jong et al., 2016), we used a more conservative approach by baseline correcting

452   each epoch from -2500 to -700 ms relative to the button press in order to avoid possible

453   contamination due to motor-related artefacts. In order to make both conditions comparable, we

454   performed the same procedure separately on the endogenous and exogenous conditions.

455   **Statistical analysis**

456   For statistical analysis of wSMI (NII), K complexity (NID), wPLI (NOI) and spectral power (NOD) on the

457   scalp EEG (29 participants) and iEEG data (1 patient), we performed repeated-measures ANOVA

458   (RANOVA) using 3 within-participant factors: condition (endogenous, exogenous), window (before

459   change, after change), and direction (one- to two-stream, two- to one-stream). Bonferroni

460   correction was computed for *post hoc* comparisons, and Bayes Factors of the null and alternative

461   hypothesis are reported (Masson 2011; Jarosz and Wiley 2014). Statistical analyses were performed

462   using Statistical Product and Service Solutions (SPSS, version 20.0, IBM), MATLAB 2018b and open-

463   source statistical software JASP (JASP Team (2017), version 0.8.1.1).

464

465   **RESULTS**

466   Twenty-nine healthy participants and one patient implanted with intracranial electrodes listened to

467   a repeating pattern of three tones followed by a temporal gap. This flow of sounds is experienced

468   either as a one-stream percept (perceptual integration) or as a two-stream percept (perceptual

469   differentiation) (Figure 1A, upper panel). Perception tends to alternate between these alternatives

470   every few seconds (Pressnitzer and Hupé 2006). Participants were asked to press a button as they

471   perceived that the one-stream percept had fully changed into the two-stream percept, and a second

472   button when perceiving the two-stream percept had fully changed into the one-stream percept

473   (Figure 1A, middle panel). As an experimental control task, we used a condition where the stimuli

474   were physically manipulated (varying the length of the silence between tones) in order to generate

475   two externally-driven alternating percepts (exogenous condition). Participants had to perform the

476   same task as in endogenous condition. This control allowed us to establish the extent to which

477   neural activity in the endogenous condition was specific to internally driven perceptual switches. It

478   also allowed us to measure typical reaction times to percept changes with known onset times (in the

479   control task), in order to determine suitable time windows for analysis. Furthermore, the exogenous

480   condition allowed us to control for top-down attention in the absence of bistability by creating

481   externally driven switches between percepts as opposed to the internally driven ones (induced

482   endogenously).

483   **Behavioural results**

484   In the endogenous condition, inter-switch duration (ISD) distributions were approximated well

485   with a gamma distribution ($P<0.001$; Figure 1B), typically reported during bistable perception

486   dynamics (e.g. Parkkonen at al., 2008). Inter-switch duration (ISD) histograms exhibited similar

487   distributions for the one- to two-stream percept and the two- to one-stream percept, with an

488   average dominance duration of 3.75 ± 0.0412 and 3.78 ± 0.0419 seconds respectively (Figure 1B).

489   No significant differences were observed between distributions ($t_{1,28}$ = 0.204; P = 0.910; Bayes

490   factor (Bf) in favour of the null = 46.19), suggesting that both directions of perceptual change

491   exhibit similar cognitive demand during internally-driven perception.

492   Similarly, in the case of the exogenous condition, discrimination of the two auditory sequences

493   showed behavioural equivalence as no differences were found in reaction times (RT) between

494   the one- to two-stream percept and the two- to one-stream percept ($t_{1,28}$ = 0.204; P = 0.840;

495   Bayes factor (Bf) in favour of the null = 4.97).

496   **Neural information integration (NII) during the endogenous and exogenous conditions**

497   We first investigated the dynamics of neural information integration in the gamma range (NII_{v}). We

498   compared activity during a 500-ms window before a perceptual change with activity after the

499   change (Figure 1A, lower panel; and see Materials and Methods). This approach contrasts with many

500   previous studies of auditory bistability (Gutschalk et al., 2005; Hill et al., 2012; Szalardy et al., 2013;

501   Billig et al. 2018; Sanders et al. 2018), where the analysis windows are time-locked to the stimulus,

502   and allowed us to concentrate on both stable and transition periods of bistable experience.

503   Response-locked analyses focused on how *ongoing* neural activity relates to perception. A repeated-

504   measures ANOVA (RANOVA; see Materials and Methods) revealed a significant triple interaction

505   between condition (endogenous, exogenous), window (before change, after change), and direction

506   (one- to two-stream, two- to one-stream) for NII$_\gamma$ ($F_{1,28}$ = 5.73, P = 0.024, η_p^2= 0.16, Bayes factor (Bf)

507   in favour of the alternative = 2.73). Bonferroni's *post hoc* test revealed higher NII$_\gamma$ in the one-stream

508   compared to the two-stream percept in the before-change (BC) window (P = 0.009, η_p^2 = 0.21, Bf in

509   favour of the alternative = 6.42) (Figure 2A, C). Interestingly, ~1 s later in the after change (AC)

510   window, NII$_\gamma$ again showed higher values for the one-stream than the two-stream percept (P =

511   0.026, η_p^2= 0.15, Bf in favour of the alternative = 2.49) (Figure 2A, C). These findings suggest that the

512   phenomenologically integrated percept consistently involved a higher level of gamma

513   neurophysiological integration than the phenomenologically differentiated one.

514   Interestingly, while NII$_\gamma$ discriminated between conscious percepts during the endogenous condition

515   (Figure 2A), it did not do so in the exogenous condition (BC: P = 0.561; Bf in favour of the null = 5.12

516   and AC: P = 0.349, Bf in favour of the null = 3.26; Bonferroni-corrected *post hoc* tests) (Figure 2B),

517   suggesting that frontoparietal NII$_\gamma$ may be specifically indexing endogenously generated percepts.

518   Furthermore, no differences were observed in the mean level of NII$_\gamma$ between endogenous and

519   exogenous conditions (main effect of condition: P = 0.248, Bf in favour of the null = 2.12) or between

520   windows (main effect of window: P = 0.918, Bf in favour of the null = 3.59), indicating that the

521   overall amount of information sharing within the frontoparietal network was similar across

522   conditions. This index of information integration was hence sensitive to endogenously driven

523   perceptual changes and may specifically underlie the formation of conscious auditory percepts.

524   In order to establish the specific role of frontoparietal signals, we computed inter-hemispheric NII$_\gamma$

525   between temporal electrodes. RANOVA found no reliable triple interaction in temporotemporal NII$_\gamma$

526   ($F_{1,28}$ = 1.51, P = 0.228, Bf in favour of the null = 2.02) (Figure 2D, E), implying relatively specific

527   involvement of frontoparietal networks in the emergence of endogenous auditory percepts. Finally,

528   and in addition to NII$_\gamma$, we investigated whether neural information integration in the alpha band

529   (NII$_\alpha$) dissociates between auditory percepts, as alpha activity has been previously related to

530   perceptual bistability (Flevaris et al., 2013; Handel and Jensen, 2014). However, the ability of

531   frontoparietal NII to track and distinguish between different endogenous percepts seems to be

532   specifically related to the gamma range since RANOVA revealed no triple interaction between

533   percepts in frontoparietal NII$_\alpha$ ($F_{1,28}$ = 1.01, P = 0.321, Bf in favour of the null = 2.48) (Figure 2F).

534   Finally, we performed *post hoc* exploratory analysis in order to further investigate NII_γ differences

535   between other electrode regions (i.e. frontofrontal, parietoparietal, temporoparietal and

536   frontotemporal pairs of electrodes). RANOVA revealed no triple interaction (condition x window x

537   direction) between these electrode clusters (Supplementary Figure 2). Similarly, we explored

538   differences between these pairs of electrodes in other canonical frequency bands (theta: NII_θ, alpha:

539   NII_α, and beta: NII_β). RANOVA revealed no significant triple interaction (condition x window x

540   direction) for the same groups of electrodes for theta (NII_θ: Supplementary Figure 3), alpha (NII_α:

541   Supplementary Figure 4) and beta bands (NII_β: Supplementary Figure 5). These exploratory results

542   further support the specific role of NII_γ in discriminating between internally-driven conscious

543   percepts.

544

545   **Neural information differentiation (NID) during the endogenous and exogenous conditions**

546   We next investigated the dynamics of neural information differentiation (NID) within frontal and

547   parietal electrodes during bistable perception (Figure 3). The RANOVA revealed a significant triple

548   interaction between condition (endogenous, exogenous), window (before change, after change),

549   and direction (one- to two-stream, two- to one-stream) for NID (P = 0.013, η_p^2 = 0.19, Bf in favour of

550   the alternative = 4.57). Bonferroni's *post hoc* test revealed higher NID in the two- compared to the

551   one-stream percept in the BC window (P = 0.011, η_p^2 = 0.20, Bf in favour of the alternative = 5.41)

552   (Figure 3A) and a similar pattern in the AC window, showing higher values for two streams than for

553   one stream (P = 0.016, Bf in favour of the alternative = 3.88, η_p^2 = 0.19) (Figure 3A). These results

554   show that the differentiated percept exhibits higher neurophysiological differentiation than the

555   integrated one.

556   As was the case for NII_γ, *post hoc* comparisons showed no NID dependence on percept in the

557   exogenous condition (B.C: P = 0.366, Bf in favour of the null = 2.66; A.C: P = 0.174, Bf in favour of the

558   null = 1.68) (Figure 3B). Furthermore, no differences were observed in the mean level of NID

559   between endogenous and exogenous conditions (main effect of condition: $F_{1,28}$ = 1.39, P = 0.248, Bf

560   in favour of the null = 2.12) or between windows (main effect of window: $F_{1,28}$ = 0.15, P = 0.228, Bf in

561   favour of the null = 3.53), indicating that the overall information differentiation within the

562   frontoparietal network was similar across conditions. Finally, no triple interaction (condition x

563   window x direction) was observed for NID between temporal electrodes (right and left hemispheres)

564   ($F_{1,28}$ = 3.59, P = 0.069; Bf in favour of the null = 0.86) (Figure 3C, D). In agreement with the NII

565   results, this index of information complexity dissociated endogenous percepts. However, NID

566   showed the opposite pattern compared to NII in terms of the direction of the effects between one

567   and two streams, suggesting that NID is capturing a different but complementary aspect of neural

568   information dynamics associated with conscious percepts.

569   Consistent with the analysis of NII, we explored NID differences between other electrode regions

570   (i.e. frontofrontal, parietoparietal, temporoparietal and frontotemporal pairs of electrodes).

571   RANOVA revealed no triple interaction (condition x window x direction) between these electrode

572   clusters (Supplementary Figure 6).

Neural information integration (NII) in human intracortical recordings

574   In order to validate these findings in a similar manner as elsewhere (Canales-Johnson et al. 2015),

575   we repeated the experiment in a patient implanted with intracranial electrodes for epilepsy surgery.

576   We benefited from the high spatial resolution of intracranial recordings, allowing us to directly test

577   the hypothesis that it is information-sharing specifically between frontal and parietal areas that

578   differentiates between the two auditory percepts. We computed NII_γ on intracranial

579   electroencephalography (iEEG) recordings between the superior parietal lobe (SPL) and middle

580   frontal gyrus (MFG), and between SPL and the orbitofrontal cortex (OF) (Table 1) obtained from the

581   intracranial patient performing the same task as above (Figure 4A-C and Supplementary Figure 8).

582   Taking the SPL-MFG and SPL-OF pairs of electrodes together, and as for the healthy participants, the

583   RANOVA showed a triple interaction between condition (endogenous, exogenous), window (before

584   change, after change), and direction (one- to two-stream, two- to one-stream) for NII_γ ($F_{1,56}$ = 45.19,

585   P < 0.001, η_p^2= 0.42, Bf in favour of the alternative > 100). Simple effects within the BC window

586   showed higher NII_γ for the one- compared to the two-stream percept in the endogenous ($F_{1,56}$ =

587   44.79, P < 0.001, η_p^2= 0.25, Bf in favour of the alternative > 100) (Figure 4B) but not the exogenous

588   condition ($F_{1,56}$ = 0.25, P = 0.517, Bf supporting the null = 4.34) (Figure 4C). In the case of the AC

589   window, the one-stream percept again showed higher NII_γ than the two-stream percept in the

590   endogenous ($F_{1,56}$ = 42.83, P < 0.001, η_p^2= 0.10, Bf supporting the alternative = 5.10) (Figure 4B) but

591   not in the exogenous condition ($F_{1,56}$ = 1.40, P = 0.731, Bf in favour of the null = 4.89) (Figure 4C).

592   In order to further test the frontoparietal specificity of the NII_γ modulation, we computed NII_γ

593   between SPL and MFG with two unrelated – as per our hypothesis - cortical areas: motor cortex

594   (MC) and posterior insular cortex (PIC) (Supplementary Figure 9). No triple interaction was observed

595   for NII_γ between SPL-MC, SPL-PIC, MFG-MC nor MFG-PIC, further confirming the spatial specificity of

596   the intracortical NII_γ results.

597   Furthermore, no differences were found between these percepts in the same iEEG recordings within

598   the alpha band (NII_α) ($F_{1,56}$ = 0.03, P = 0.853, Bf in favour of the null = 7.24) (Figure 4F, G). Individual

599 SPL-MFG and SPL-OF pairs for NII_γ and NII_α are depicted in Supplementary Figure 8 and

600 Supplementary Figure 10, respectively. Finally, and in agreement with the scalp EEG results, a

601 further iEEG exploratory analysis revealed no triple interaction (RANOVA: condition x window x

602 direction) between SPL-MFG and SPL-OF electrodes in the theta (NII_θ: Supplementary Figure 11), nor

603 beta (NII_β: Supplementary Figure 12) bands.

604

605 **Neural information differentiation (NID) in human intracortical recordings**

606 Next, we investigated NID dynamics on iEEG signals in the intracranial patient within SPL, MFG and

607 OF (Figure 4D, E). Again, RANOVA showed a triple interaction between (endogenous, exogenous),

608 window (before change, after change), and direction (one- to two-stream, two- to one-stream) ($F_{1,56}$

609 = 24.96, $P < 0.001$, η_p^2 = 0.25, Bf in favour of the alternative = 10.02). In agreement with the scalp EEG

610 results, a simple effects analysis within the BC window showed higher NID for the

611 phenomenologically differentiated percept compared to the phenomenologically integrated percept

612 in the endogenous ($F_{1,56}$ = 19.08, $P < 0.001$, η_p^2 = 0.42, Bf in favour of the alternative > 100) (Figure

613 4D) but not in the exogenous condition ($F_{1,56}$ = 1.92, $P = 0.171$, Bf in favour of the null = 1.94) (Figure

614 4E). In the case of the AC window, the two-stream percept again showed higher NID than the one-

615 stream percept in the endogenous ($F_{1,56}$ = 10.57, $P = 0.003$, η_p^2 = 0.28, Bf in favour of the alternative =

616 20.15) (Figure 4D) but not in the control (exogenous) condition ($F_{1,56}$ = 0.25, $P = 0.615$, Bf in favour of

617 the null = 4.82) (Figure 7E). These findings demonstrate strong convergent evidence between scalp

618 EEG and direct cortical recordings, further supporting the hypothesis that phenomenology goes

619 along with neurophysiology of conscious percepts, specifically indexed by frontoparietal ongoing

620 activity. Individual SPL-MFG and SPL-OF pairs for NID are depicted in Supplementary Figure 13.

621 **Neural oscillatory integration (NOI) in the endogenous and exogenous conditions**

622 We next evaluated the theoretical prediction that information dynamics but not oscillatory dynamics

623 of brain activity underpins the emergence of internally-driven percepts (Koch et al. 2016). Thus, we

624 investigated whether neural oscillatory integration (NOI) of ongoing activity might also capture the

625 dynamics of auditory bistability. Specifically, we investigated whether frontoparietal gamma phase

626 synchronization (Weighted Phase-Lag Index ($wPLI_\gamma$)) could differentiate between endogenous

627 percepts. Unlike for NII_γ, RANOVA revealed no triple interaction between condition (endogenous,

628 exogenous), window (before change, after change), and direction (one- to two-stream, two- to one-

629 stream) for NOI_γ ($F_{(1,28)}$ = 0.12, $P = 0.726$, Bf in favour of the null = 3.58) (Figure 5A,B). However, a

630 weak interaction between condition (endogenous, exogenous) and window (before change, after

631 change) was found ($F_{(1,28)}$ = 4.22, $P = 0.049$, Cohen's $d = 0.77$, Bf in favour of the alternative = 1.50)

632 (Figure 5C,D). Bonferroni's *post hoc* test showed that NOI_v significantly decreased in the AC window

633 compared to the BC window in the endogenous ($P = 0.016$, $\eta_p^2 = 0.17$, Bf in favour of the alternative =

634 3.73) (Figure 5C) but probably not in the exogenous condition ($P = 0.236$, Bf in favour of the null =

635 2.04) (Figure 5D).

636 Furthermore, the same null result for NOI_v between directions was observed in the intracranial

637 patient (RANOVA (condition x window x direction): $F_{(1,56)} = 0.12$; $P = 0.726$, Bf in favour of the null =

638 4.73) (Figure 5E,F). As with the scalp EEG, the intracranial patient showed an interaction between

639 condition and window ($F_{(1,56)} = 13.51$, $P = 0.001$, $\eta_p^2 = 0.19$, Bf in favour of the alternative = 68.09) in

640 NOI_v, showing a decrease in phase synchrony in the AC window compared to the BC window only in

641 the endogenous condition (Bonferroni's *post hoc* test in endogenous condition: $P = 0.001$, $\eta_p^2 = 0.18$,

642 Bf in favour of the alternative = 53.48; and exogenous condition: $P = 0.147$, Bf in favour of the null =

643 1.92) (Figure 5G,H) between SPL and MFG-OF electrodes. These findings suggest that oscillatory

644 integration does not index the identity of auditory percepts but may relate to percept stability:

645 phase synchrony maxima occur in the BC window (before the end of a stable percept) and phase

646 synchrony minima in the AC window (just at the onset of percept stability).

647 **Neural oscillatory power (NOP) in the endogenous and exogenous conditions**

648 We finally performed an exploratory analysis aiming at investigating the neural differences during

649 exogenously-driven perception. In order to evaluate the neural response on electrodes sensitive to

650 auditory perturbations, we analysed the neural oscillatory power (NOI) in the same gamma band as

651 previous analyses but focusing on the temporal and parietal electrodes. In the exogenous condition

652 we expected higher gamma spectral power during the integrated ('ABA-') as compared to the

653 differentiated ('AB--') pattern since the former contains one more tone than the latter, potentially

654 eliciting a greater neural response. RANOVA revealed an interaction between condition

655 (endogenous, exogenous), window (before change, after change) and direction (one- to two-stream,

656 two-to one-stream) for NOP ($F_{(1,28)} = 4.30$, $P = 0.047$, $\eta_p^2 = 0.13$, Bf in favour of the alternative = 4.67)

657 (Figure 6). Bonferroni's *post hoc* test revealed differences in the exogenous condition in line with our

658 prediction. NOP was higher in the one- compared to the two-stream percept in the BC window ($F_{(1,28)}$

659 $= 6.37$, $P = 0.001$, $\eta_p^2 = 0.032$, Bf in favour of the alternative = 6.45) (Figure 6) and a similar pattern

660 held in the AC window, with larger values for one stream than for two streams ($P = 0.001$, Bf in

661 favour of the alternative = 7.88, $\eta_p^2 = 0.002$) (Figure 6B). No differences in NOP were observed

662 between conscious percepts in the endogenous condition (B.C: $P = 0.845$, Bf in favour of the null =

663 8.13; $P = 0.453$, Bf in favour of the null = 6.17) (Figure 6A). These results suggest that spectral power

664 within temporal and parietal electrodes is sufficient for indexing conscious percepts when these are

665   externally-driven, that is, when the two patterns (i.e. integrated and differentiated) were physically

666   present in the auditory stimuli.

667

668   **DISCUSSION**

669   Here we demonstrate that frontoparietal information dynamics dissociate alternative conscious

670   percepts during internally but not externally driven percepts. By studying the neural dynamics (EEG

671   and direct cortical recordings) of theoretically-motivated information metrics, we show that

672   empirically tractable measures of neural information integration and neural information

673   differentiation map auditory percepts experienced either as perceptually integrated (one-stream) or

674   differentiated (two-stream), respectively. Furthermore, phase synchronization of oscillatory gamma

675   activity in the frontoparietal network does not differentiate between auditory percepts, nor does

676   the information between temporal networks. Finally, when perception was driven externally (no

677   bistability, control condition) by a change in the sound stream, neural oscillatory power

678   distinguished between percepts but information measures did not.

679   ***Neural correlates of consciousness and the instantiation of meaningful signatures of information***

680   ***integration and differentiation.***

681   Our results expand the understanding of the neural correlates of consciousness (NCC) (Koch et al.

682   2016) in several ways. First, our experimental findings directly support information-based theories of

683   consciousness (Dehaene and Changeux 2011; Dehaene et al. 2014; Tononi et al. 2016); in their

684   current instantiation, the Integrated Information Theory (IIT) (Tononi et al. 2016) and the Global

685   Neuronal Workspace Theory (GNWT) (Dehaene and Changeux 2011) of consciousness both

686   emphasize the role of information exchange in generating conscious percepts. Although both

687   theories conceptualize information differently, their proposed empirical indices are based on the

688   classical Shannon-entropy information framework. Using these measures of information dynamics,

689   our results show convergent evidence supporting both GNWT and IIT predictions by demonstrating a

690   role of neural information in the emergence of contents of consciousness. However, the

691   interpretation of these results in light of the IIT and GNWT is somewhat different.

692   The GNWT provides a framework for evaluating the process of becoming aware of a percept (i.e. the

693   conscious access for a stimulus), specifically in our case the experience of perceiving one or two

694   auditory streams. Of the proposed key features of neural processing that the GNWT supports is the

695   modulation of frontoparietal networks when gaining conscious awareness. This is why we set out to

696   test the frontoparietal network at the electrode level (EEG) and the intracranial cortical level (iEEG).

697   In its original conception, the GNWT did not specifically proposed integration measures that would

698   be neural signatures of gain of conscious awareness. Later on, however, in a landmark paper Gaillard

699   et al in 2009 showed connectivity and granger-causality calculations that signalled the access to

700   consciousness in a masking paradigm in intracranial patients (Gaillard et al., 2009). Echoing the need

701   to better define what a putative measure of brain integration is, we searched for those measures

702   that could be used to assess integration information and differentiation in the time dynamics of the

703   stream of consciousness of the current task.

704   Although most of IIT's empirical work has been focused on finding proxy measures for distinguishing

705   levels of consciousness (e.g. wakefulness versus sleep), recent efforts have been put in investigating

706   perceptual integration and differentiation at the first-person, phenomenological level using time-

707   resolved experimental paradigms (Boly at al., 2015). We think that this current framework allows for

708   testing the concepts of integration and differentiation in the context of the study of the first-person,

709   content of consciousness (i.e. hearing one-stream vs two-stream stimuli) rather than on the study of

710   the third-person, state of consciousness (e.g. being awake vs being asleep). We believe our study

711   substantially improves this approach for three main reasons. First, the repertoire of conscious

712   contents is controlled (i.e. one vs two auditory streams). Second, the physical stimulation remains

713   constant while perception does not. Finally, our EEG/iEEG information metrics possess higher

714   temporal resolution than those used in fMRI studies, allowing the finely-grained characterization of

715   the phenomenology of conscious contents.

716   It is in this respect that we think that concepts taken from both theoretical frameworks (GNWT and

717   IIT) are useful to explain some cognitive process that we believe are at play in bistable perception.

718   We do not claim that this unifies the theories, but that it is possible to make use of parts of them to

719   frame results that can help understanding the neural signatures of contents of consciousness. An

720   important caveat of this conceptualization is that the theoretical argumentations from GNWT and IIT

721   do not make explicit predictions about the possible differences between internally and externally

722   driven contents of consciousness, while we explicitly test this difference.

723   Our results suggest a differential role of information integration vs. information differentiation in the

724   emergence of conscious percepts from those proposed before. According to IIT, the neural activity

725   associated with conscious percepts should reflect the joint presence of neurophysiological

726   integration and neurophysiological differentiation. Under this theoretical framework, integration is

727   expected – in principle – to be paralleled by differentiation of neural activity. Contrary to this

728   prediction, our results show dissociation between neurophysiological integration and

729   neurophysiological differentiation of frontoparietal ongoing activity. Interestingly, while the

730   phenomenologically integrated percept (one-stream) showed a relative increase in NII and relative

731   decrease in NID, the perceptually differentiated percept (two-stream) exhibited the opposite

732   pattern, that is, a decrease in NII and increase in NID. Together, these dissociated patterns suggest

733   that each measure is instead directly associated with the phenomenology of internally-driven

734   conscious percepts: whereas information integration of neural activity is capturing

735   phenomenological integration (one-stream percept), information differentiation may be capturing

736   phenomenological differentiation (two-stream percept).

737   ***Neural signatures of the emergence of internally- and externally-driven conscious contents.***

738   We have demonstrated a potential mechanistic role of information integration and differentiation in

739   the formation of endogenous percepts. Why do information metrics capture the neural dynamics of

740   internally-driven conscious percepts? Coordination in the brain has been classically studied by

741   computing phase synchronization between neural oscillations (Uhlhaas et al. 2009; Engel et al.

742   2013). Synchronization is a highly-ordered form of neural coordination that primarily captures the

743   linear (or proportional) phase relationship between signals at specific frequencies (phase-locking).

744   Thus, a mechanism of coordination-by-synchrony captures only certain regimes of neural

745   coordination that are periodic. However, brain dynamics exhibit both a tendency to integrate

746   information (synchronization) and a tendency for the components to differentiate information

747   (independent function) (Dehaene and Changeux 2011; Tognoli and Kelso 2014; Tononi et al. 2016).

748   During auditory bistability, conscious percepts typically alternate continuously without becoming

749   locked into any one percept for long periods. We propose that underlying this dynamical process are

750   ensembles of neurons that are repeatedly assembled and disassembled, and that this non-trivial

751   dynamic might be instantiated by a mechanism of coding-by-information that captures complex,

752   nonlinear patterns of neural activity and not merely simple proportional associations between

753   neural signals. In fact, we have recently shown that wSMI (NII) performs better at capturing highly

754   non-linear interactions than wPLI (NOI) between long-distance neural signals by using realistic brain

755   simulations (Imperatori et al., 2019).

756   Contrasting the emergence of internally-driven conscious percepts, the two auditory sequences

757   presented during the exogenous conditions were distinguished by a difference in spectral power in

758   the gamma band. The difference was observed mainly in the temporoparietal electrodes and the

759   direction of the effect is consistent with the idea that an extra tone in the sequence elicited a higher

760   neural response, i.e. that the ABA- sequence showed higher gamma power than the AB-- sequence.

761   Thus, contrary to the information-theory metrics, we suggest that the spectral gamma power

762   response is linearly (or proportionally) related to the physical characteristics of the stimulus itself

763　(exogenous condition), and not to the internal interpretation of the bistable sequence, as no

764　differences were observed in the endogenous condition. Hence for the exogenous condition, while

765　the report is the same (one or two streams), the neural signatures point a different process in the

766　brain when the nature of the contents differs.

767　***Conscious auditory percepts and ongoing neural activity.***

768　The frontoparietal patterns of neural information are a manifestation of the interaction between the

769　external stimulation and endogenous, ongoing brain activity, as opposed to activation purely

770　imposed by the auditory stimuli. Thus, NII and NID patterns do not merely reflect stimulus-driven

771　neural activity but rather the intrinsic coordination of endogenous frontoparietal neural activity.

772　Indeed, in the endogenous condition of our study, internally generated changes in neural activity

773　were associated with changes in conscious percepts in the complete absence of any change in the

774　auditory stimuli. In line with our results, recent studies in the visual system have shown that long-

775　distance integration of ongoing oscillations reflects internally coordinated activity associated with

776　conscious perception (Hipp et al. 2012; Engel et al. 2013; Helfrich et al. 2016). Here, by directly

777　measuring the amount of information integration and information differentiation contained in the

778　ongoing neural activity, we demonstrate a functional role of information dynamics in the emergence

779　of auditory conscious percepts. Our approach provides a framework for examining whether this

780　relationship between neural and perceptual integration and differentiation generalizes, for example

781　to the perception of ambiguous stimuli in other sensory modalities, or across modalities.

782　Although the pioneering electrophysiological studies supporting the active role of ongoing activity in

783　perception and cognition date from the 70's (Freeman 1976, 2000), over the last decade ongoing

784　brain activity has been mainly studied in the context of "resting state networks" (Fox and Raichle

785　2007). In these recent studies, fluctuations in ongoing activity between spatially segregated

786　networks (brain regions) are correlated when a participant is not performing an explicitly defined

787　task. In the present study, by taking advantage of the high temporal resolution of EEG and direct

788　cortical recordings, we show that patterns of neural information are transiently coordinated during

789　the active discrimination of internally generated auditory percepts. Furthermore, our results also

790　allowed us to differentiate the contribution of information in frequency-space, showing that gamma

791　but not alpha NII differentiates auditory percepts during bistable perception.

792　***Auditory bistable perception and frontoparietal activity.***

793　Our results also suggest a fruitful new approach to conceptualizing and investigating bistable

794　auditory perception. We demonstrate that the dynamics of auditory endogenous percepts can be

795   associated with long-distance coordination of neural activity. For the ABA- patterns presented here,

796   while both one-stream and two-stream percepts depend on the integration of tones over time, the

797   latter also requires integration across tone frequency. We argue that this additional integration may

798   draw on, or be reflected in, an increase in information sharing in ongoing frontoparietal neural

799   activity. Additionally, maintenance of two distinct perceptual streams of sounds was associated with

800   more differentiated neural patterns than when a single stream was perceived. How these findings

801   relate to previous demonstrations of greater stimulus-locked activity in auditory cortex (Gutschalk et

802   al. 2005; Hill et al. 2011; Szalardy et al. 2013; Billig et al. 2018; Sanders et al. 2018) and greater BOLD

803   response in intraparietal sulcus (Cusack 2005; Hill et al. 2011) for two streams is presently unclear.

804   However, the involvement of neural circuits extending beyond sensory regions in parsing the

805   auditory environment is not surprising given that attention switching (Billig and Carlyon 2016),

806   linguistic knowledge (Billig et al. 2013), and predictability (Winkler and Schröger 2015) have been

807   shown to affect auditory streaming.

808   These findings provide convergent evidence about the role of frontoparietal networks in the

809   dynamics of formation and maintenance of internally-driven conscious contents. Research in visual

810   bistability has focused on characterizing content-related activity predominantly in local brain areas

811   or networks (Sterzer et al. 2009). Of those few studies that have expanded their scope to associative

812   cortices and wider networks, one has recently proposed mechanistic accounts on visual percepts

813   using multivariate pattern analysis (MVPA) of fMRI data (Wang et al. 2013). The results showed

814   differential patterns of BOLD activity in high-order frontoparietal regions between visual percepts

815   during bistable perception. The present study complements these results by showing a role for the

816   frontoparietal network in indexing percepts in the auditory modality. Furthermore, the temporal

817   resolution of our EEG and iEEG data enabled us to characterize the fine-grained temporal dynamics

818   of neural information integration associated with specific auditory percepts within the frontoparietal

819   network. These results represent convergent evidence towards a possible general mechanism of

820   information integration underlying the emergence of the contents of consciousness under invariant

821   stimulation.

822   In conclusion, we have presented experimental evidence that conscious percepts may be supported

823   by different neural mechanisms depending on whether they are internally or externally driven. We

824   have highlighted the stark contrast between fleeting endogenous percepts, where neural integration

825   and differentiation parallel the corresponding integrated and differentiated percepts, and those that

826   are externally triggered, for which no differences between information-theory measures were

827   observed. However, when conscious percepts are driven by changes in the external stimulation,

828   fluctuations in spectral power are sufficient for indexing perceptual integration and differentiation.

829   Importantly, the conceptual mapping between phenomenology and the neurophysiology that we

830   have highlighted here should be considered as a fruitful approach for measuring the different

831   dimensions of phenomenology in an experimentally testable manner. In light of some of the main

832   current theoretical frameworks of conscious perception -IIT and GNWT- we provide additional

833   experimental scaffolding to further understand what we have in mind at any given time.

834

835

836

837

838

839

840

841

842   **FIGURES**

843
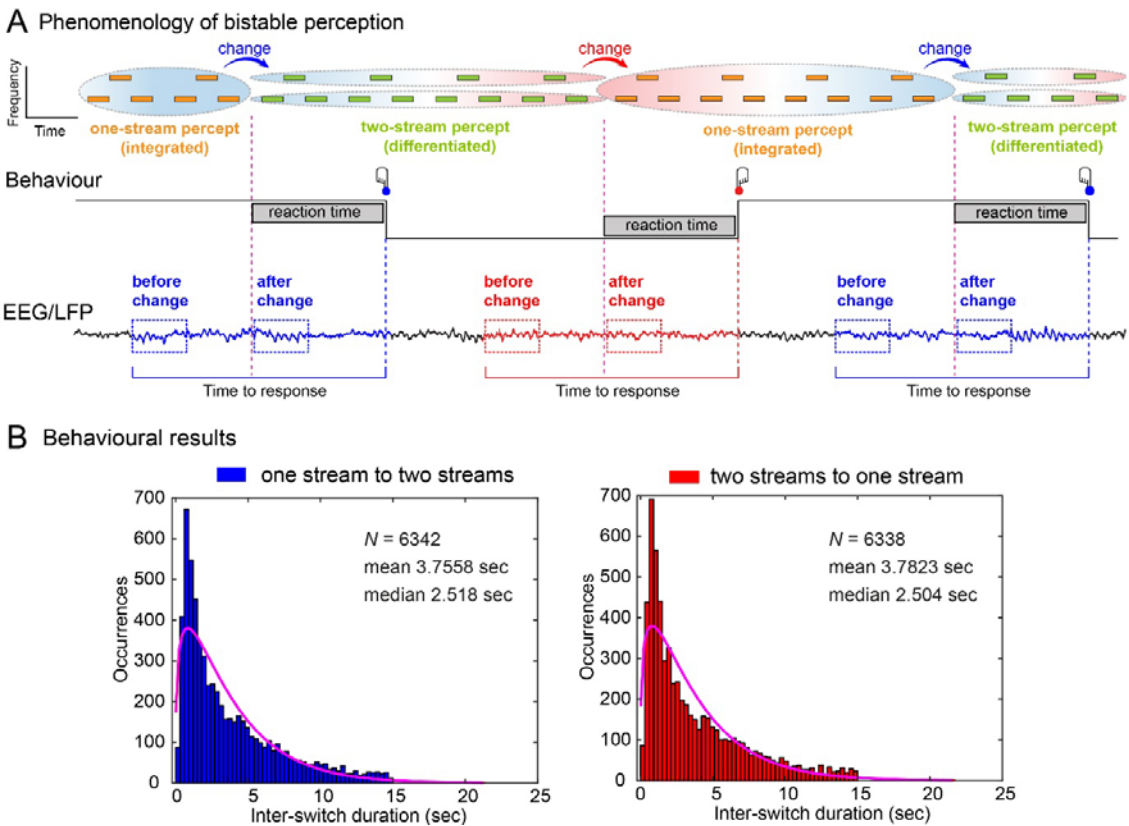
844 **Figure 1. Experimental design and analysis of ongoing brain activity. (A)** *Top row*: Phenomenology

845 (reported experience) during auditory bistability. Participants listened to a series of tones of two

846 different frequencies separated by a temporal gap (see Experimental Procedures). Tones are

847 experienced either as one stream (phenomenologically integrated percept; orange blocks

848 surrounded by one ellipse) or as two streams (phenomenologically differentiated percept; green

849 blocks surrounded by two ellipses). Perceptual transitions occur either in the one-stream to two-

850 stream direction (blue arrows and blue background) or in the two-stream to one-stream direction

851 (red arrow and red background). *Middle row*: behavioural responses during the task. Participants

852 pressed one button when perceiving that one stream had fully changed into the two-stream percept

853 (blue button) and another button when perceiving that two streams had fully changed into the one-

854 stream percept (red button). *Bottom row*: dynamical analyses and windows of interest for EEG and

855 iEEG signal analyses. Ongoing activity in during both transitions was calculated using a sliding

856 window procedure over a fixed time window locked to the onset of the button press. Window size

857 was calculated based on the mean reaction times (RT) in the exogenous condition (1342 ms), and

858 the minimum duration between responses that guaranteed no overlap between epochs (2500 ms)

859 (see Materials and Methods). **(B)** *Left panel*: Inter-switch duration histograms for the one- to two-

860 stream perceptual stable period and for the two- to one-stream perceptual stable period (*Right*

861 *panel*).

862

863

864

865

866

867

868

869

870

871

872

873

874

875

876
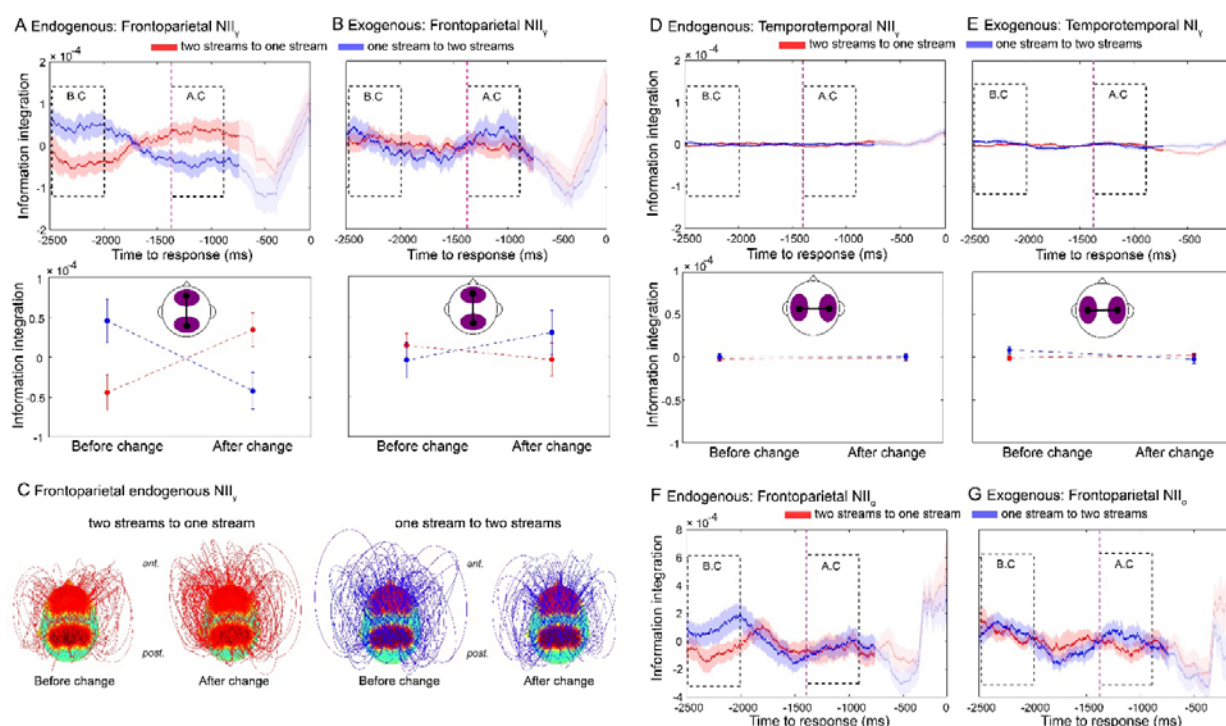
Figure 2. Frontoparietal NII dissociates alternative endogenous percepts during bistable perception. Neural dynamics of NII_v for transitions from the two-stream to the one-stream percept (red line) and from the one-stream to the two-stream percept (blue line) for the endogenous **(A)** and exogenous (control) conditions **(B)**. Purple dashed line marks the mean reaction time (1342 ms) of the exogenous (control) condition. Auditory percepts were directly compared in two windows of interest: the before-change (BC) and the after-change (AC) windows. **(C)** Connectivity topographies for the BC and AC windows for transitions from the two-stream to the one-stream percept (left panel) and from the one-stream to the two-stream percept (right panel) averaged over participants in the endogenous condition. Red areas on the scalp indicate regions of interest (frontal and parietal electrodes, see Experimental Procedures). The height of an arc connecting two nodes indicates the strength of the NII link between them. Values are time-locked to the button press (0 ms) and baseline corrected between -2500 and -700 ms relative to button press (see Materials and Methods). Statistical analyses (bottom row) were computed on two pre-defined 500 ms windows: a BC window (-2500 to 2000 ms) and an AC window (-1342 ms to -842 ms). The onset of both windows was defined based on a control (exogenous) condition in which the stimuli physically change to generate two different percepts (see Experimental Procedures). Shaded bars (top row) and error bars (middle row) represent s.e.m. **(D, E)** Temporotemporal NII in the endogenous and exogenous

894   conditions. **(F, G)** Frontoparietal NII in the alpha band (NII_α) during endogenous **(F)** and exogenous

895   **(G)** conditions.

896

897

898
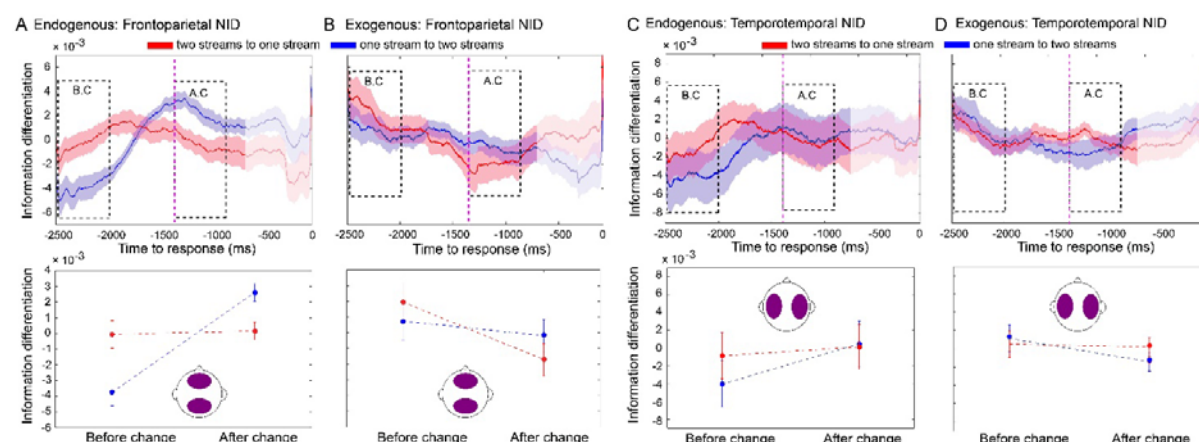
899   **Figure 3. Frontoparietal NID dissociates alternative endogenous percepts during bistable**

900   **perception**. Neural dynamics of NID from the two-stream to the one-stream percept (red line) and

901   from the one-stream to the two-stream percept (blue line) for the endogenous **(A)** and exogenous

902   (control) conditions **(B)**. **(C, D)** Temporotemporal NID dynamics for the endogenous **(C)** and

903   exogenous (control) conditions **(D)**. Purple dashed line marks the mean reaction time (1342 ms) of

904   the exogenous (control) condition. Statistical analysis was performed as described in Figure 2.

905   Shaded bars (top row) and error bars (bottom row) represent s.e.m.

906

907
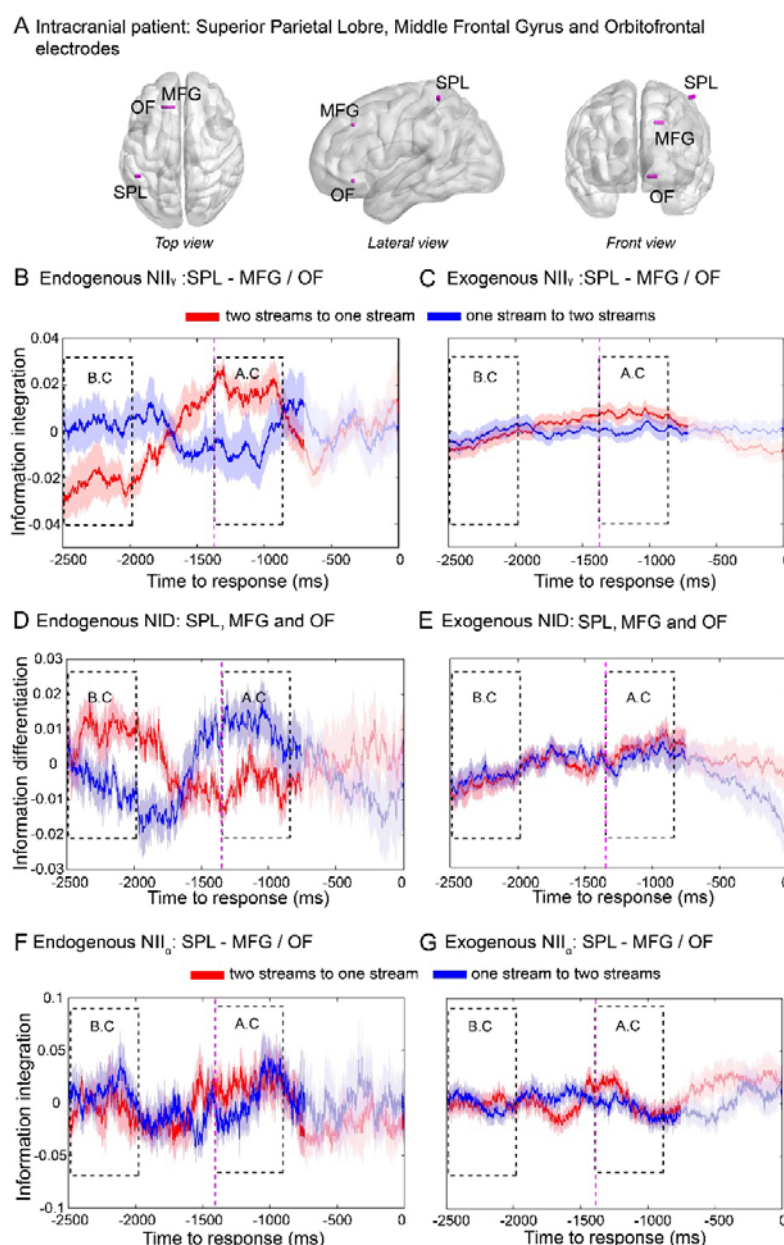
Figure 4. Frontoparietal NII and NID in intracranial recordings. (a) Electrodes were implanted in the left superior parietal lobe (SPL), left middle frontal gyrus (MFG) and left orbitofrontal cortex (OF) (Table 1). Representative pair of electrodes (SPL-MFG) showing NII_γ and NID of transitions from the two-stream to the one-stream percept (red line) and from the one-stream to the two-stream percept (blue line) in the endogenous **(B, D)** and exogenous **(C, E)** conditions, respectively. **(F, G)** Frontoparietal NII in the alpha band (NII_α) in intracranial recordings for the endogenous **(F)** and exogenous condition **(G)**. Purple dashed line marks the mean reaction time (1380 ms) of the exogenous (control) condition of the intracranial data. Statistical analyses were performed as explained in Figure 2. Shaded bars represent s.e.m.

917

918
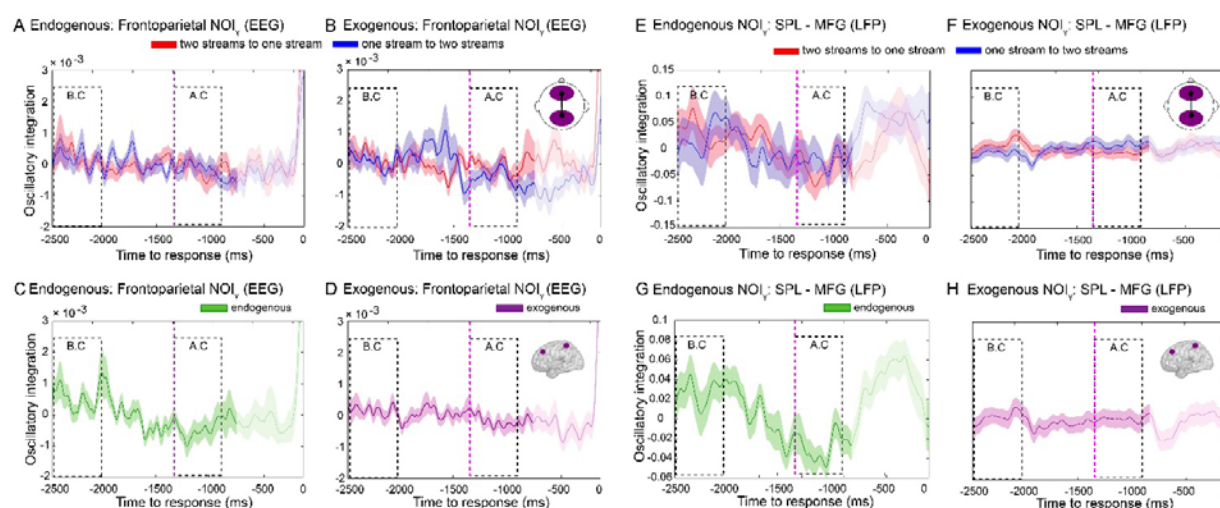
Figure 5. Frontoparietal NOI in the endogenous and exogenous conditions. Dynamics of ongoing NOI_γ from the two-stream to the one-stream percept (red line) and from the one-stream to the two-stream percept (blue line) for the endogenous **(A)** and exogenous **(B)** conditions. Ongoing NOI_γ during transitions in both directions in the endogenous **(C)** and exogenous **(D)**. Statistical analyses were performed as described in Figure 2. Shaded bars represent s.e.m. **(E-H)** Frontoparietal NOI in the alpha band (NOI_γ) in intracranial recordings. Ongoing NOI_γ during transitions in both directions **(E, F)** in the endogenous **(C)** and exogenous **(D)**. Statistical analyses were performed as described in Figure 2. Error bars represent s.e.m.

927

928

929

930

931

932

933

934

935

936
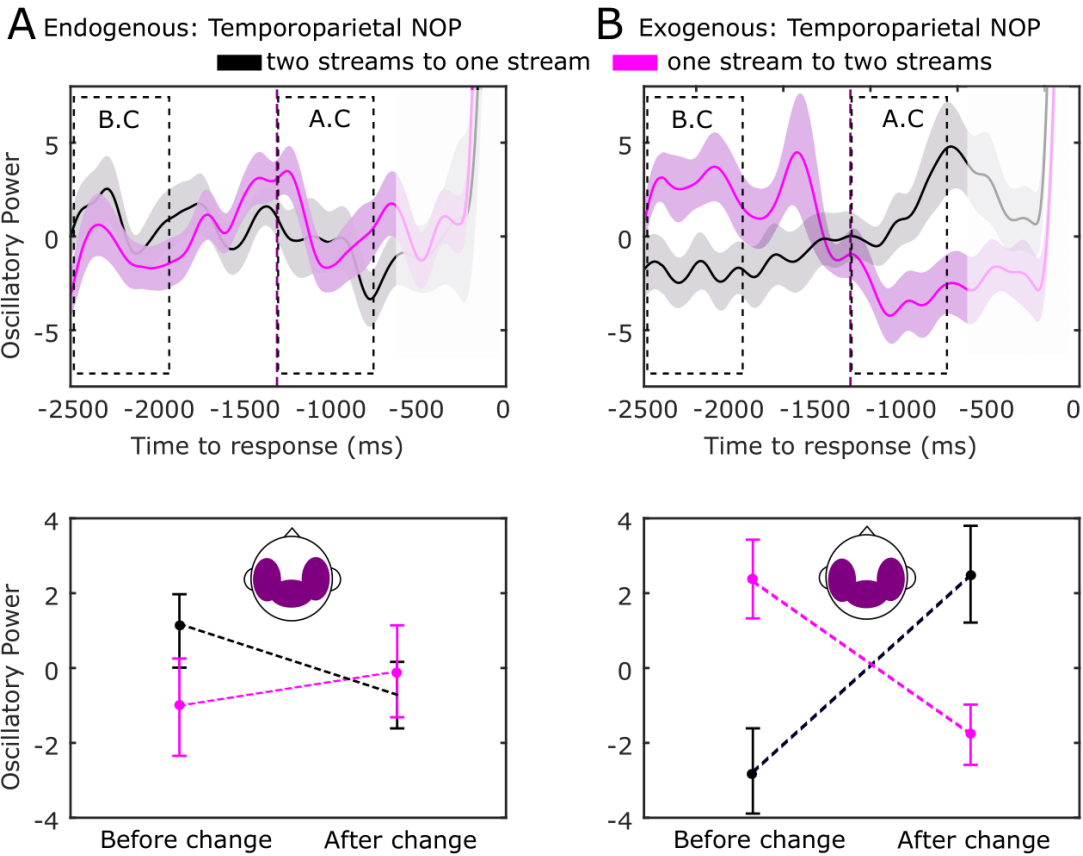
Figure 6. Temporoparietal NOP in the gamma range dissociates alternative exogenous percepts. Neural dynamics of NOP from the two-stream to the one-stream percept (black line) and from the one-stream to the two-stream percept (purple line) for the endogenous **(A)** and exogenous (control) conditions **(B)**. Purple dashed line marks the mean reaction time (1342 ms) of the exogenous (control) condition. Statistical analysis was performed as described in Figure 2. Shaded bars (top row) and error bars (bottom row) represent s.e.m.

952 **Table 1. Coordinates and anatomical loci of intracranial electrodes analysed**

Electrode	MNI Coordinates	Cortical region (gyrus)
1	-26; -44; 62	Left Superior Parietal Lobe
2	-28; -44; 62	Left Superior Parietal Lobe
3	-30; -44; 62	White Matter
4	-14; 32; 40	Left Middle Frontal Gyrus
5	-17; 32; 40	Left Middle Frontal Gyrus
6	-20; 32; 40	Left Middle Frontal Gyrus
7	-12; 32; 40	White Matter
8	-8; 32; -10	Left Orbitofrontal Cortex
9	-11; 32; -10	Left Orbitofrontal Cortex
10	-14; 32; -10	Left Orbitofrontal Cortex
11	-16; 32; 10	White Matter
12	-26; -28; 62	Left Primary Motor Cortex
13	-13; -28; 62	White Matter
14	-40; -8; 4	Left Posterior Insular Cortex
15	-40; -30; 4	White Matter

953 Note: Electrodes are depicted in Figure 4 and Supplementary Figures 8 to 13. SPL = Superior Parietal

954 Lobe. MFG = Middle Frontal Gyrus. OF = Orbitofrontal Cortex. MC = Motor Cortex. PIC = Posterior

955 Insular Cortex.

956

957

958

959

960

961

962

963

964

965   **REFERENCES**

966   Basirat A, Sato M, Schwartz JL, Kahane P, Lachaux JP. 2008. Parieto-frontal gamma band activity
967   during the perceptual emergence of speech forms. Neuroimage. 42:404–413.

968   Billig AJ, Carlyon RP. 2016. Automaticity and Primacy of Auditory Streaming: Concurrent Subjective
969   and Objective Measures. J Exp Psychol Hum Percept Perform. 42:339-353

970   Billig AJ, Davis MH, Carlyon RP. 2018. Neural decoding of bistable sounds reveals an effect of
971   intention on perceptual organization. J Neurosci. 38:2844-2853

972   Billig AJ, Davis MH, Deeks JM, Monstrey J, Carlyon RP. 2013. Lexical influences on auditory
973   streaming. Curr Biol. 23:1585–1589.

974   Boly M, Sasai S, Gosseries O, Oizumi M, Casali A, Massimini M, Tononi G. 2015. Stimulus set
975   meaningfulness and neurophysiological differentiation: A functional magnetic resonance
976   imaging study. PLoS One. 10.

977   Canales-Johnson A, Silva C, Huepe D, Rivera-Rei Alvaro, Noreika V, Del Carmen Garcia M, Silva W,
978   Ciraolo C, Vaucheret E, Sedeno L, Couto B, Kargieman L, Baglivo F, Sigman M, Chennu S, Ibanez
979   A, Rodriguez E, Bekinschtein TA. 2015. Auditory feedback differentially modulates behavioral
980   and neural markers of objective and subjective performance when tapping to your heartbeat.
981   Cereb Cortex. 25:4490–4503.

982   Carlyon RP, Cusack R, Foxton JM, Robertson IH. 2001. Effects of attention and unilateral neglect on
983   auditory stream segregation. J Exp Psychol Hum Percept Perform. 27:115–127.

984   Casali AG, Gosseries O, Rosanova M, Boly M, Sarasso S, Casali KR, Casarotto S, Bruno M-A, Laureys S,
985   Tononi G, Massimini M. 2013. A Theoretically Based Index of Consciousness Independent of
986   Sensory Processing and Behavior. Sci Transl Med. 5:198ra105-198ra105.

987   Chaitin GJ. 1974. Information-theoretic computation complexity. IEEE Trans Inf Theory. 20:10–15.

988   Chaitin GJ. 1995. The berry paradox. Complex Syst Bin Networks. 461:23–31.

989   Chennu S, Finoia P, Kamau E, Allanson J, Williams GB, Monti MM, Noreika V, Arnatkeviciute A,
990   Canales-Johnson A, Olivares F, Cabezas-Soto D, Menon DK, Pickard JD, Owen AM, Bekinschtein
991   TA. 2014. Spectral Signatures of Reorganised Brain Networks in Disorders of Consciousness.
992   PLoS Comput Biol. 10.

993   Cusack R. 2005. The intraparietal sulcus and perceptual organization. J Cogn Neurosci. 17:641–651.

994   De Jong MC, Hendriks RJM, Vansteense MJ, Raemaekers M, Verstraten FAJ, Ramsey NF, Erkelens CJ,

995   Leijten FSS, Van Ee R. 2016. Intracranial recordings of occipital cortex responses to illusory

996   visual events. J Neurosci. 36:6297–6311.

997   Dehaene S, Changeux JP. 2011. Experimental and Theoretical Approaches to Conscious Processing.

998   Neuron.

999   Dehaene S, Charles L, King JR, Marti S. 2014. Toward a computational theory of conscious

1000   processing. Curr Opin Neurobiol.

1001   Delorme A, Makeig S. 2004. EEGLAB: an open source toolbox for analysis of single-trial EEG dynamics

1002   including independent component analysis. J Neurosci Methods. 134:9–21.

1003   Doesburg SM, Kitajo K, Ward LM. 2005. Increased gamma-band synchrony precedes switching of

1004   conscious perceptual objects in binocular rivalry. Neuroreport. 16:1139–1142.

1005   Engel A K, Fries P, Singer W. 2001. Dynamic predictions: oscillations and synchrony in top-down

1006   processing. Nat Rev Neurosci. 2:704–716.

1007   Engel AK, Gerloff C, Hilgetag CC, Nolte G. 2013. Intrinsic Coupling Modes: Multiscale Interactions in

1008   Ongoing Brain Activity. Neuron.

1009   Fahrenfort, JJ, Snijders, TM, Heinen K, van Gaal S, Scholte HS, Lamme, V. A. F. (2012). Neuronal

1010   integration in visual cortex elevates face category tuning to conscious face perception. Proc

1011   Natl Acad Sci. 109: 21504–21509.

1012   Fahrenfort JJ, van Leeuwen J, Olivers CNL, Hogendoorn H. (2017). Perceptual integration without

1013   conscious access. Proc Natl Acad Sci. 114: 3744–3749.

1014   Fesi JD, Mendola JD. 2015. Individual peak gamma frequency predicts switch rate in perceptual

1015   rivalry. Hum Brain Mapp. 36:566–576.

1016   Flevaris A V, Martínez A, Hillyard S a. 2013. Neural substrates of perceptual integration during

1017   bistable object perception. J Vis. 13:17.

1018   Foster BL, He BJ, Honey CJ, Jerbi K, Maier A, Saalmann YB. 2016. Spontaneous Neural Dynamics and

1019   Multi-scale Network Organization. Front Syst Neurosci. 10:7.

1020   Fox MD, Raichle ME. 2007. Spontaneous fluctuations in brain activity observed with functional

1021   magnetic resonance imaging. Nat Rev Neurosci. 8:700–711.

1022   Frässle S, Sommer J, Jansen A, Naber M, Einhäuser W. 2014. Binocular rivalry: frontal activity relates

1023   to introspection and action but not to perception. J Neurosci. 34:1738–1747.

1024   Freeman W. 2000. Neurodynamics: An Exploration in Mesoscopic Brain Dynamics, Perspectives in
1025   Neural Computing. Springer London.

1026   Freeman WJ. 1976. Mass action in the nervous system. Neuroscience. 1:423.

1027   Freeman WJ. 2015. Mechanism and significance of global coherence in scalp EEG. Curr Opin
1028   Neurobiol. 31:199–205.

1029   Friston KJ. 2006. Statistical Parametric Mapping: The Analysis of Functional Brain Images, Functional
1030   neuroimaging: Technical.

1031   Gutschalk A, Micheyl C, Melcher JR, Rupp A, Scherg M, Oxenham AJ. 2005. Neuromagnetic correlates
1032   of streaming in human auditory cortex. J Neurosci. 25:5382–5388.

1033   Handel BF, Jensen O. 2014. Spontaneous local alpha oscillations predict motion-induced blindness.
1034   Eur J Neurosci.

1035   Helfrich RF, Knepper H, Nolte G, Sengelmann M, König P, Schneider TR, Engel AK. 2016. Spectral
1036   fingerprints of large-scale cortical dynamics during ambiguous motion perception. Hum Brain
1037   Mapp.

1038   Hill KT, Bishop CW, Yadav D, Miller LM. 2011. Pattern of BOLD signal in auditory cortex relates
1039   acoustic response to perceptual streaming. BMC Neurosci. 12:85.

1040   Hipp JF, Hawellek DJ, Corbetta M, Siegel M, Engel AK. 2012. Large-scale cortical correlation structure
1041   of spontaneous oscillatory activity. Nat Neurosci. 15:884–890.

1042   Imperatori LS, Betta M, Cecchetti L, Canales-Johnson A, Ricciardi E, Siclari F, Pietrini P, Chennu S,
1043   Bernardi G. 2019. EEG functional connectivity metrics wPLI and wSMI account for d distinct
1044   types of brain functional interactions. Sci Rep 9: 8894.

1045   Jarosz AF, Wiley J. 2014. What are the odds? A practical guide to computing and reporting Bayes
1046   factors. J Probl Solving. 7:2.

1047   King JR, Sitt JD, Faugeras F, Rohaut B, El Karoui I, Cohen L, Naccache L, Dehaene S. 2013. Information
1048   sharing in the brain indexes consciousness in noncommunicative patients. Curr Biol. 23:1914–
1049   1919.

1050   Koch C, Massimini M, Boly M, Tononi G. 2016. Neural correlates of consciousness: progress and
1051   problems. Nat Rev Neurosci. 17:307–321.

1052 Kolmogorov AN. 1965. Three approaches to the definition of the concept of quantity of information.
1053   IEEE Trans Inf Theory.

1054 Lachaux JP, Rodriguez E, Martinerie J, Varela FJ. 1999. Measuring phase synchrony in brain signals.
1055   Hum Brain Mapp. 8:194–208.

1056 Le Van Quyen M, Foucher J, Lachaux J, Rodriguez E, Lutz a, Martinerie J, Varela FJ. 2001. Comparison
1057   of Hilbert transform and wavelet methods for the analysis of neuronal synchrony. J Neurosci
1058   Methods. 111:83–98.

1059 Li G, Jiang S, Paraskevopoulou SE, Wang M, Xu Y, Wu Z, Chen L, Zhang D, Schalk G. 2018. Optimal
1060   referencing for stereo-electroencephalographic (SEEG) recordings. Neuroimage. 183:327–335.

1061 Lempel A, Ziev J. 1976. On the Complexity of Finite Sequences. IEEE Trans Inf Theory. 22:75–82.

1062 Levy J, Vidal JR, Fries P, Démonet J-F, Goldstein A, Demonet J-F, Goldstein A. 2015. Selective Neural
1063   Synchrony Suppression as a Forward Gatekeeper to Piecemeal Conscious Perception. Cereb
1064   Cortex. 1–13.

1065 Masson MEJ. 2011. A tutorial on a practical Bayesian alternative to null-hypothesis significance
1066   testing. Behav Res Methods. 43:679–690.

1067 Melloni L, Molina C, Pena M, Torres D, Singer W, Rodriguez E. 2007. Synchronization of neural
1068   activity across cortical areas correlates with conscious perception. J Neurosci. 27:2858–2865.

1069 Noreika V, Canales-Johnson A, Koh J, Taylor M, Massey I, Bekinschtein TA. 2015. Intrusions of a
1070   drowsy mind: Neural markers of phenomenological unpredictability. Front Psychol. 6.

1071 Oizumi M, Albantakis L, Tononi G. 2014. From the Phenomenology to the Mechanisms of
1072   Consciousness: Integrated Information Theory 3.0. PLoS Comput Biol. 10.

1073 Oostenveld R, Fries P, Maris E, Schoffelen JM. 2011. FieldTrip: Open source software for advanced
1074   analysis of MEG, EEG, and invasive electrophysiological data. Comput Intell Neurosci. 2011.

1075 Parkkonen L, Andersson J, Hämäläinen M, Hari R. 2008. Early visual brain areas reflect the percept of
1076   an ambiguous scene. Proc Natl Acad Sci U S A. 105:20500–20504.

1077 Pressnitzer D, Hupé JM. 2006. Temporal Dynamics of Auditory and Visual Bistability Reveal Common
1078   Principles of Perceptual Organization. Curr Biol. 16:1351–1357.

1079 Rorden C, Brett M. 2000. Stereotaxic Display of Brain Lesions. Behav Neurol. 12:191–200.

1080 Salomon D. 2004. Data compression: the complete reference. Springer Science & Business Media.

1081   Sanders RD, Winston JS, Barnes GR, Reis G. 2018. Magnetoencephalographic correlates of
1082   perceptual state during auditory bistability. Sci Reports. 8:976.

1083   Schartner M, Seth A, Noirhomme Q, Boly M, Bruno MA, Laureys S, Barrett A. 2015. Complexity of
1084   multi-dimensional spontaneous EEG decreases during propofol induced general anaesthesia.
1085   PLoS One. 10.

1086   Schartner MM, Carhart-Harris RL, Barrett AB, Seth AK, Muthukumaraswamy SD. 2017. Increased
1087   spontaneous MEG signal diversity for psychoactive doses of ketamine, LSD and psilocybin. Sci
1088   Rep. 7.

1089   Sitt JD, King JR, El Karoui I, Rohaut B, Faugeras F, Gramfort A, Cohen L, Sigman M, Dehaene S,
1090   Naccache L. 2014. Large scale screening of neural signatures of consciousness in patients in a
1091   vegetative or minimally conscious state. Brain. 137:2258–2270.

1092   Snyder JS, Gregg MK, Weintraub DM, Alain C. 2012. Attention, awareness, and the perception of
1093   auditory scenes. Atten Conscious Differ senses. 95.

1094   Stam CJ, Nolte G, Daffertshofer A. 2007. Phase lag index: Assessment of functional connectivity from
1095   multi channel EEG and MEG with diminished bias from common sources. Hum Brain Mapp.
1096   28:1178–1193.

1097   Sterzer P, Kleinschmidt A, Rees G. 2009. The neural bases of multistable perception. Trends Cogn Sci.

1098   Szalardy O, Bohm TM, Bendixen A, Winkler I. 2013. Event-related potential correlates of sound
1099   organization: Early sensory and late cognitive effects. Biol Psychol. 93:97–104.

1100   Tognoli E, Kelso JAS. 2014. The Metastable Brain. Neuron.

1101   Tononi G, Boly M, Massimini M, Koch C. 2016. Integrated information theory: from consciousness to
1102   its physical substrate. Nat Rev Neurosci. 17:450–461.

1103   Uhlhaas PJ, Pipa G, Lima B, Melloni L, Neuenschwander S, Nikolic D, Singer W. 2009. Neural
1104   synchrony in cortical networks: history, concept and current status. Front Integr Neurosci. 3:17.

1105   Varela F, Lachaux JP, Rodriguez E, Martinerie J. 2001. The brainweb: phase synchronization and
1106   large-scale integration. Nat Rev, Neurosci. 2:229–239.

1107   Vinck M, Oostenveld R, Van Wingerden M, Battaglia F, Pennartz CMA. 2011. An improved index of
1108   phase-synchronization for electrophysiological data in the presence of volume-conduction,
1109   noise and sample-size bias. Neuroimage. 55:1548–1565.

1110   Wang M, Arteaga D, He BJ. 2013. Brain mechanisms for simple perception and bistable perception.

1111   Proc Natl Acad Sci. 110:E3350–E3359.

1112   Winkler I, Schröger E. 2015. Auditory perceptual objects as generative models: Setting the stage for

1113   communication by sound. Brain Lang. 148:1–22.

1114   Xia M, Wang J, He Y. 2013. BrainNet Viewer: A Network Visualization Tool for Human Brain

1115   Connectomics. PLoS One. 8.